Supplementary Information

Fabrication and Understanding of Cu_3Si-Si@Carbon@Graphene Nanocomposites as High-performance Anode for Lithium-Ion Batteries

Zhiming Zheng[a,#], Hong-Hui Wu[b,#], Huixin Chen[c], Yong Cheng[a], Qiaobao Zhang[a,*], Qingshui Xie[a], Laisen Wang[a], Kaili Zhang[d], Ming-Sheng Wang[a], Dong-Liang Peng [a,*], Xiao Cheng Zeng [b,*]

[a] Department of Materials Science and Engineering, Collaborative Innovation Center of Chemistry for Energy Materials, Xiamen University, Xiamen, Fujian 361005, China

[b] Department of Chemistry, University of Nebraska-Lincoln, NE 68588 Lincoln, United States

[c]Xiamen Institute of Rare Earth Materials, Haixi institutes, Chinese Academy of Sciences, Xiamen 361024, China

[d] Department of Mechanical and Biomedical Engineering, City University of Hong Kong, 83 Tat Chee Avenue, Hong Kong

[*]Corresponding authors: Qiaobao Zhang (zhangqiaobao@xmu.edu.cn), Dong-Liang Peng(dlpeng@xmu.edu.cn) and Xiao Cheng Zeng (xzeng1@unl.edu).

# These authors contributed equally to this work.

The agglomeration of SC nanoparticles is shown by the FESEM images in Fig. S1a and S1b, which are completely enfolded by graphene, forming a well-connected 3D conductive network. The TEM image in Fig. S1c further shows that the SC nanoparticles around 35-45 nm in diameter with regular and uniform structure encapsulated into some pieces of graphene sheets. A high-resolution TEM (HRTEM) image in the Fig. S1d presents the carbon shells of SC composites around 3-4 nm in thickness. The inset image in Fig. S1d depicts clear and continuous lattice-fringe with the neighboring fringes distance is about 0.314 nm, which corresponds to that of (111) lattice spacing of Si. The STEM image and the corresponding element mappings of SCG are displayed in Supplementary Fig. S1e-h, respectively. The clear distribution of C and Si elementals further confirms the encapsulation of SC composites in graphene sheets.

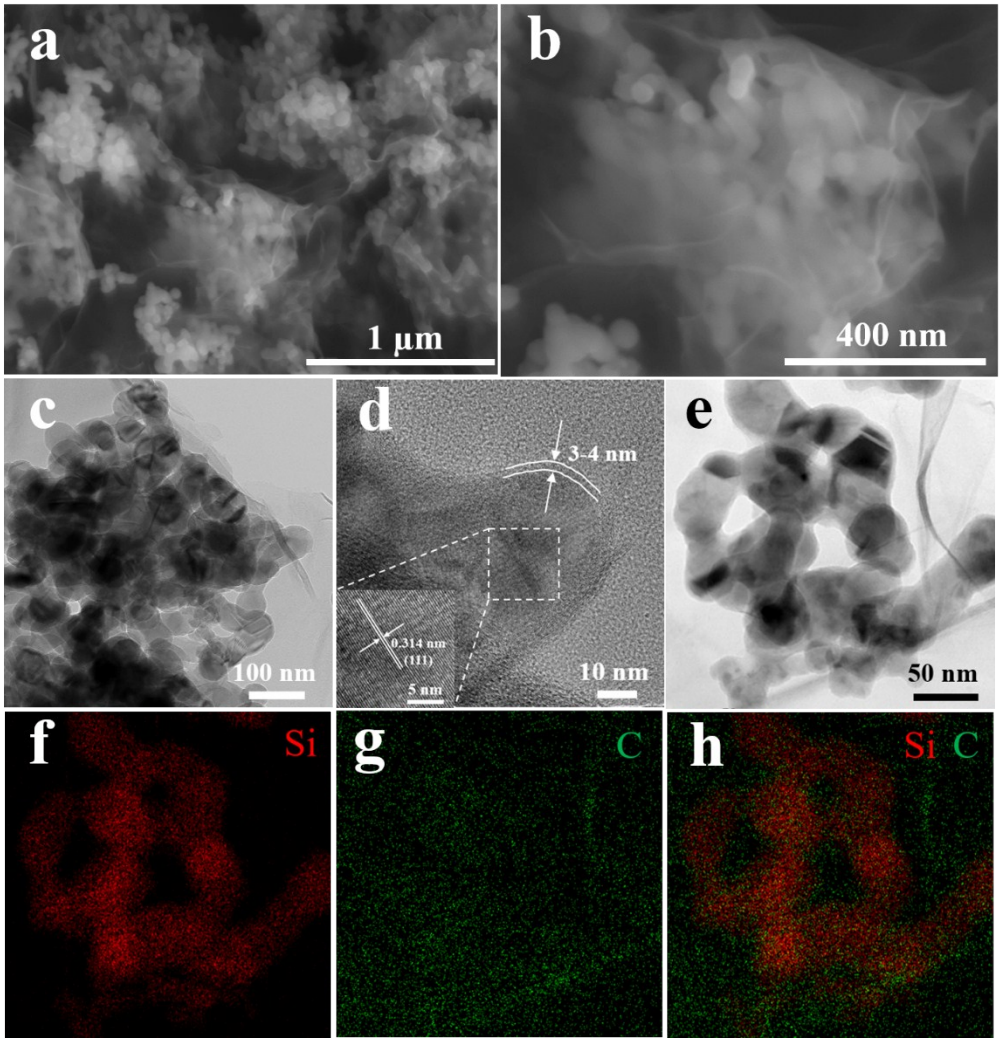

Fig. S1 (a, b) FESEM images of SCG composite. (c)TEM and (d) HRTEM image of SCG composite. (e -h) STEM image of SCG composite and corresponding element mappings of Si and C elements.

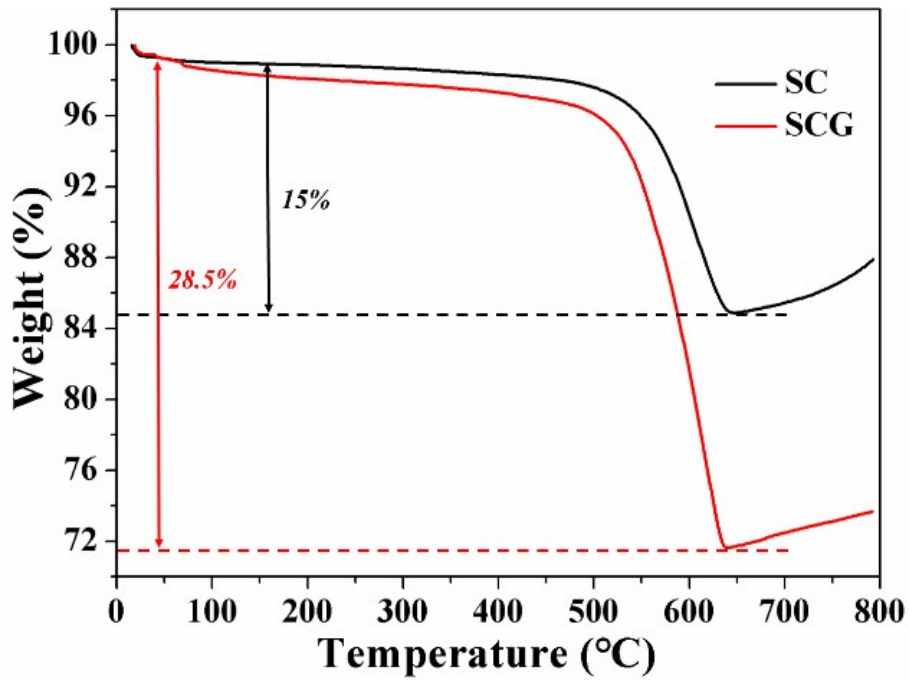

Fig. S2 Thermal analysis of SC and SCG composites.

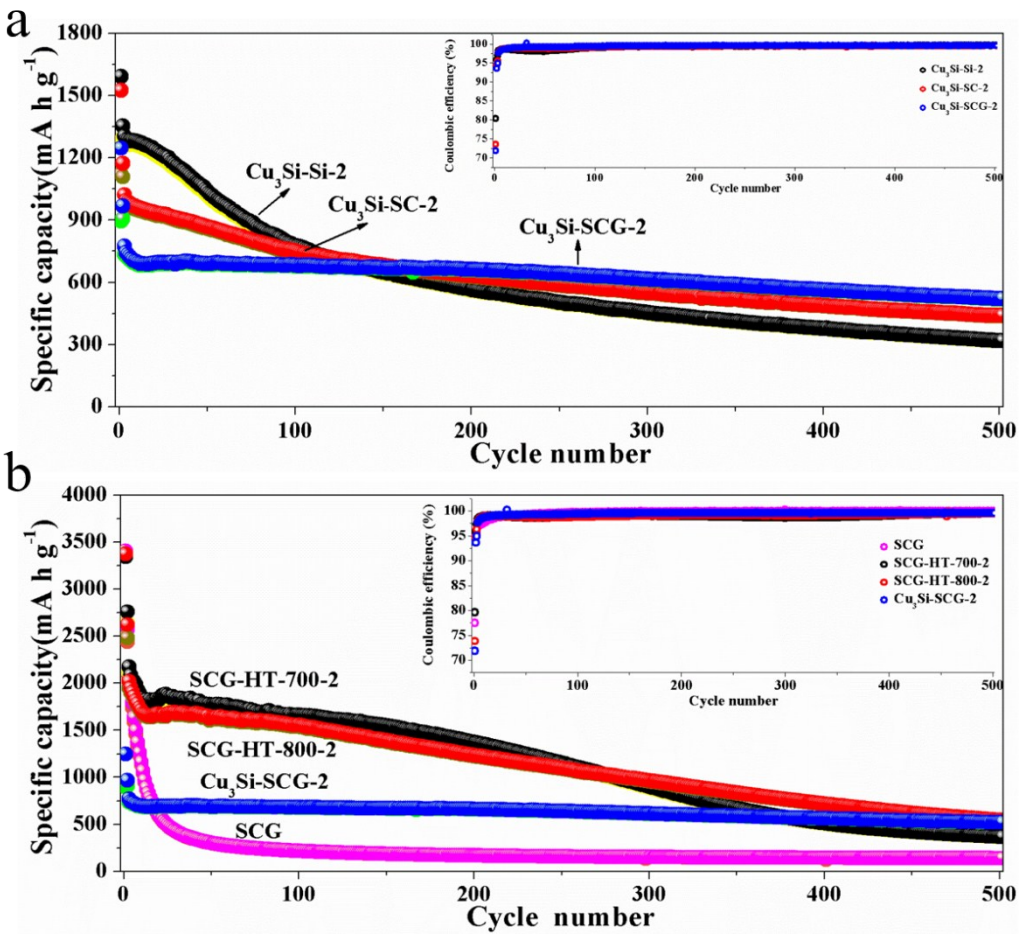

Fig. S3 (a) Cycling performance of Cu_3Si-Si-2, Cu_3Si-SC-2 and Cu_3Si-SCG-2 composite at current density of 1 A g^{-1}. (b) Cycling performance of SCG together with SCG composite after heat treatment 2 h at 700, 800 and 900 °C at current density of 1 A g^{-1}

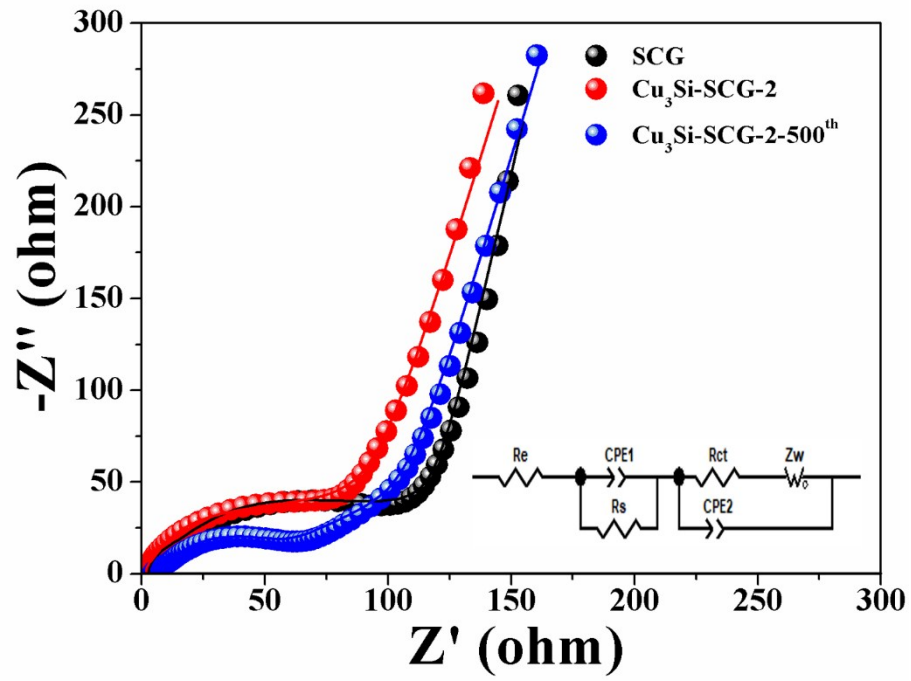

Fig. S4 Experimental (scatter diagram) and fitted (solid lines) Nyquist plots of SCG electrode before cycling, Cu_3Si-SCG -2 electrode before cycling, Cu_3Si-SCG-2 electrode after 500 cycles at 4 A g^{-1}.

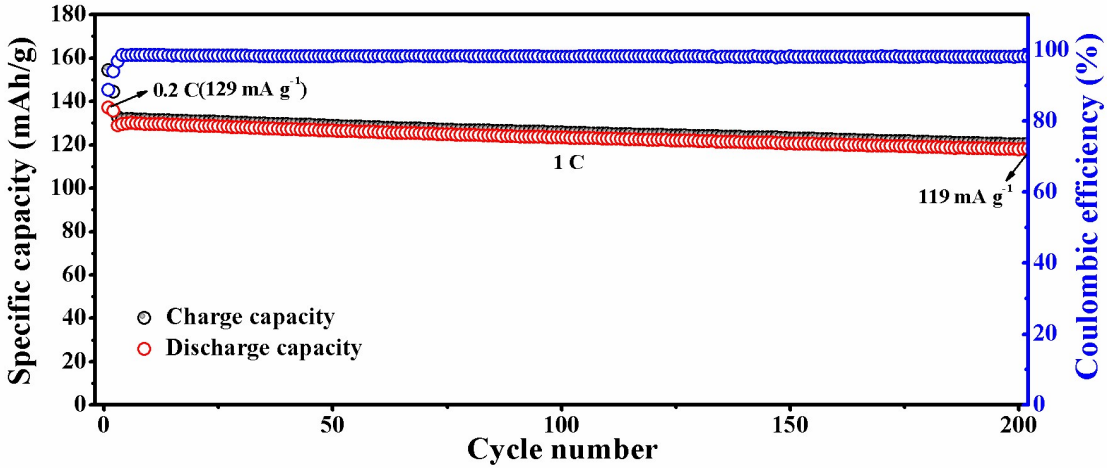

Fig. S5**.** Cycling performance of the LCO cathode in half cell: at 1 C rate for 200 cycles.

Table S1 A summary of the performances of different inactive phase/Si-based anodes in the literature in comparison with the results in this work.

Electrode material	**Cycling stability**				
	Capacity after cycles [mA h g^{-1}]	**cycle**	**Current density [A g^{-1}]**	**Capacity retention [%]**	**Ref.**
Highly connected hollow Si-Cu alloy-nanotube	1676	100	0.84	77.6	1
Micro-sized FeCuSi ternary composites	1054	50	0.5C	90	2
Nanoporous Si/Cu composites	1306.2	150	0.2	55.6	3
Si–Ti–Ni alloy	900 (based on Si–Ti–Ni alloy)	50	1C	_	4
Antimony-doped tin oxide coated Si	1320	50	0.5C	88	5
Si_{SERE}	1186.9	180	1.5	_	6
Cu_3Si@Si core–shell nanoparticles	1560.6	50	1	89.2	7
Si-Cu_3Si-Al_2O_3 nanocomposite	704	200	0.2	83.7	8
Cu_3Si-SCG-2	**522 (based on the total mass of Cu_3Si-SCG)**	**500**	**1**	**70.7**	**This work**
Cu_3Si-SCG-2	**483 (based on the total mass of Cu_3Si-SCG)**	**500**	**4**	**80**	**This work**
Cu_3Si-SCG-2	**676 (based on the mass of Cu_3Si and Si)**	**500**	**4**	**80**	**This work**
Cu_3Si-SCG-2	**1208 (based on the mass of Si)**	**500**	**4**	**80**	**This work**

References

1. H. Song, H. X. Wang, Z. Lin, X. Jiang, L. Yu, J. Xu, Z. Yu, X. Zhang, Y. Liu, P. He, L. Pan, Y. Shi, H. Zhou and K. Chen, Highly Connected Silicon-Copper Alloy Mixture Nanotubes as High-Rate and Durable

Anode Materials for Lithium-Ion Batteries, *Adv. Funct. Mater.*, 2016, **26**, 524-531.

2. S. Chae, M. Ko, S. Park, N. Kim, J. Ma and J. Cho, Micron-sized Fe-Cu-Si ternary composite anodes for high energy Li-ion batteries, *Energy Environ. Sci.*, 2016, **9**, 1251-1257.
3. C. Xu, Q. Hao and D. Zhao, Facile fabrication of a nanoporous Si/Cu composite and its application as a high-performance anode in lithium-ion batteries, *Nano Research*, 2016, **9**, 908-916.
4. S.-B. Son, S. C. Kim, C. S. Kang, T. A. Yersak, Y.-C. Kim, C.-G. Lee, S.-H. Moon, J. S. Cho, J. T. Moon, K. H. Oh and S.-H. Lee, A Highly Reversible Nano-Si Anode Enabled by Mechanical Confinement in an Electrochemically Activated $Li_xTi_4Ni_4Si_7$ Matrix, *Adv. Energy Mater.*, 2012, **2**, 1226-1231.
5. J. L. Lee, E.-H. Lee, J.-H. Park, S. Park and S.-Y. Lee, Ultrahigh-Energy-Density Lithium-Ion Batteries Based on a High-Capacity Anode and a High-Voltage Cathode with an Electroconductive Nanoparticle Shell, *Adv. Energy Mater.*, 2014, **4**, 1301542.
6. W. Ma, X. Liu, X. Wang, Z. Wang, R. Zhang, Z. Yuan and Y. Ding, Crystalline Cu-silicide stabilizes the performance of a high capacity Si-based Li-ion battery anode, *J. Mater. Chem. A*, 2016, **4**, 19140-19146.
7. J. Zhou, N. Lin, Y. Han, J. Zhou, Y. Zhu, J. Du and Y. Qian, Cu3Si@Si core-shell nanoparticles synthesized using a solid-state reaction and their performance as anode materials for lithium ion batteries, *Nanoscale*, 2015, **7**, 15075-15079.
8. S. O. Kim and A. Manthiram, Low-cost carbon-coated Si-Cu_3Si-Al_2O_3 nanocomposite anodes for high-performance lithium-ion batteries, J. Power Sources, 2016, 332, 222-229.